**Supplementary Table S1.** The correlation coefficients of APTw intensity and semi-quantitative ($Path_{spec}$, $Cell_{spec}$, and $Nec_{spec}$) and quantitative ($Cell_{count}$ and Ki-67) pathologic indices

| | $Path_{spec}$ | $Cell_{spec}$ | $Nec_{spec}$ | $Cell_{count}$ | Ki-67 |
|---|---|---|---|---|---|
| APTw Intensity | 0.651*** | 0.616*** | -0.255* | 0.580*** | 0.458*** |
| $Path_{spec}$ | | 0.675*** | -0.286** | 0.622*** | 0.380** |
| $Cell_{spec}$ | | | -0.174 | 0.725*** | 0.495*** |
| $Nec_{spec}$ | | | | -0.066 | -0.085 |
| $Cell_{count}$ | | | | | 0.587*** |

Note: Path = histopathologic assignment; Cell = cellularity; Nec = necrosis. Subscript "spec" means the specimen-based measurement from the whole specimen, and $Cell_{count}$ and Ki-67 were quantitatively counted by image processing software semi-automatically. For $Path_{spec}$, we used: quiescent = 1; mixed = 2; and active = 3. For the sake of simplicity, four no tumor-containing specimens were grouped with quiescent tumor specimens for the analysis. * $P < 0.05$; ** $P < 0.01$; *** $P < 0.001$.

## Supplementary Results

### Regression Analysis between APTw and Pathologic Indices

We finally performed a multiple linear regression analysis to model the relationship between APTw signal intensity and pathologic indices. We tested three potential predictor sets: [$Path_{spec}$, $Cell_{spec}$, $Nec_{spec}$, Ki-67], [$Path_{spec}$, $Cell_{count}$, $Nec_{spec}$, Ki-67], and [$Path_{spec}$, $Cell_{spec}$, $Nec_{spec}$, $Cell_{count}$, Ki-67]. For $Path_{spec}$, we used: quiescent = 1; mixed = 2; and active = 3. Four no tumor-containing specimens were grouped with quiescent tumor specimens for the analysis. After a stepwise elimination, the same model equation was obtained:

$$APTw = 0.620 + 0.812 \times Path_{spec} + 1.280 \times Ki\text{-}67 \; (R^2 = 0.546; P < 0.05). \quad [S1]$$

The histopathologic assignment ($Path_{spec}$: active, mixed, quiescent/no tumor) was identified as the most powerful factor that affected APTw signal intensity, followed by the Ki-67 index. These results indicated that APTw imaging can identify areas with the most malignant biological behavior, consistent with active tumor within heterogeneous brain lesions.

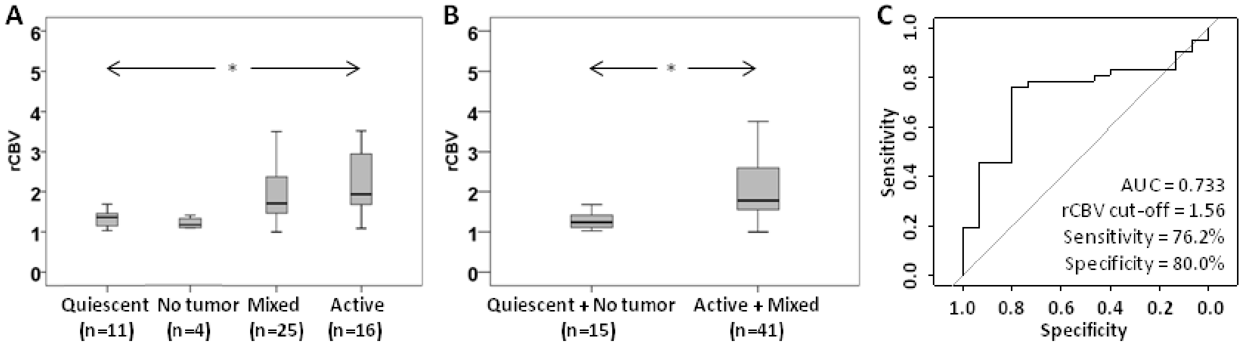


**Supplementary Fig. S1.** Quantitative analysis and diagnostic ability of rCBV. **A,** Quantitative comparison of rCBV intensities that correspond to quiescent, mixed, and active specimens, as well as non-tumor specimens. **B,** Quantitative comparison of rCBV intensities that correspond to treatment effects (non-tumor and quiescent) and tumor recurrence (mixed and active). **C,** The ROC analysis of rCBV intensities as an imaging biomarker to distinguish active glioma from treatment effects. * $P < 0.05$.

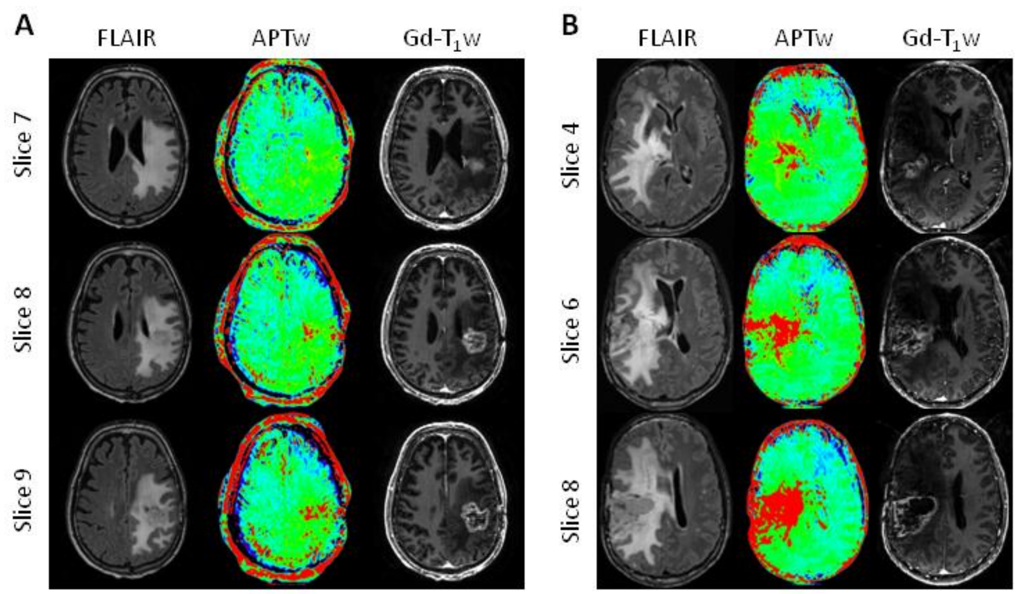


**Supplementary Fig. S2.** Anatomical and APTw MR images for a patient with treatment effect (**A,** Patient 17) and a patient with recurrent tumor (**B,** Patient 2). Only 3/15 slices acquired were shown. Areas with recurrent tumor (namely, APTw > 1.79%, compared with CNAWM) were marked in red, which were used to calculate the APTw-based recurrent tumor volume ($Vol_{APTw}$).

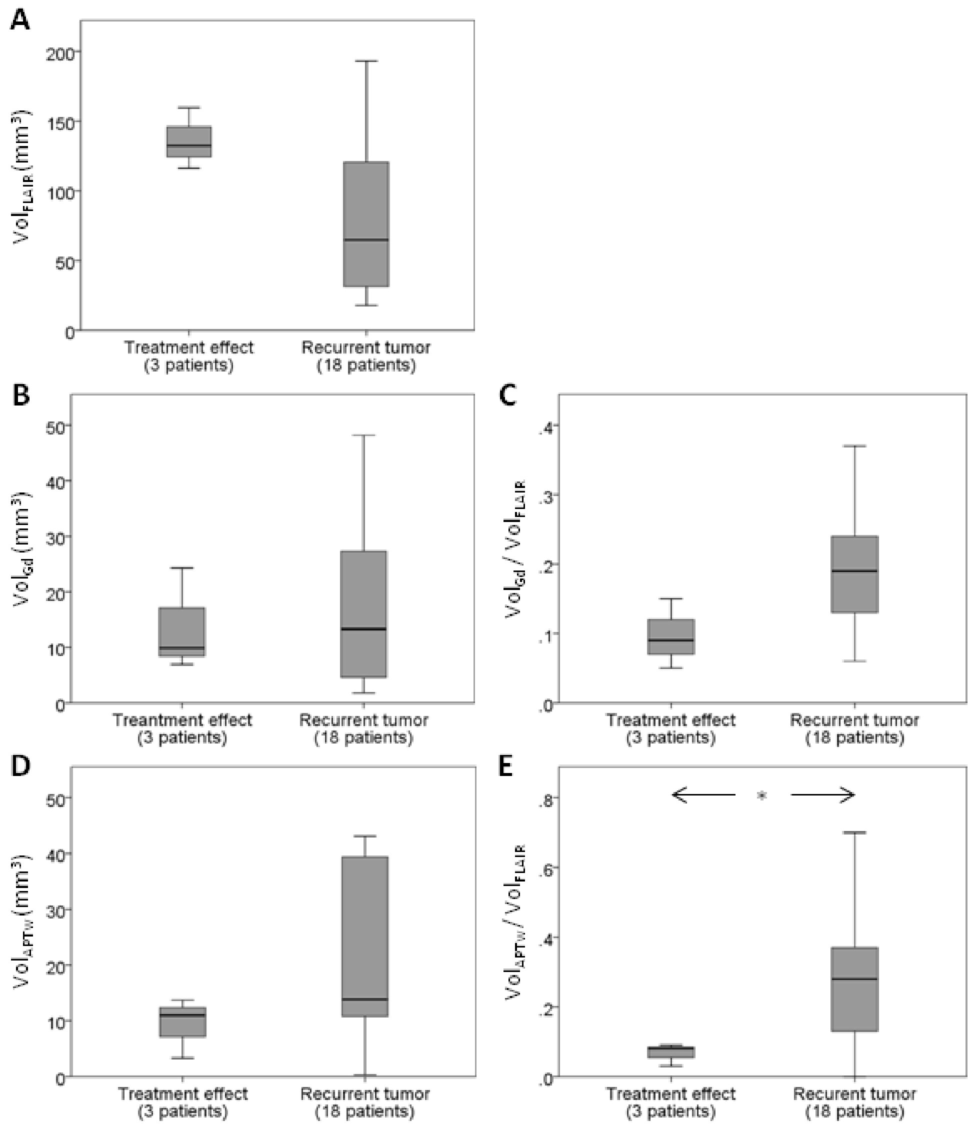


**Supplementary Fig. S3.** Comparison between tumor volumes for three patients with treatment effects and 18 patients with recurrent tumor. **A,** FLAIR hyperintensity-based tumor volumes ($Vol_{FLAIR}$). **B,** Gd-enhancing tumor volumes ($Vol_{Gd}$). **C,** $Vol_{Gd}/Vol_{FLAIR}$. **D,** APTw-based recurrent tumor volume (namely, APTw > 1.79%, compared with CNAWM; $Vol_{APTw}$). **E,** $Vol_{APTw}/Vol_{FLAIR}$. Based on the Mann-Whitney U test, the mean tumor volumes of FLAIR hyperintensity and Gd enhancement were not significantly different between these two patient groups. However, the relative APTw-based recurrent tumor volumes ($Vol_{APTw}/Vol_{FLAIR}$) were significantly lower for three patients with treatment effects than for 18 patients with recurrent tumor (0.07 ± 0.03 vs. 0.31 ± 0.25; $P < 0.05$).